Journal of Materials Chemistry A

A Robust and Ion-Conductive Protein-Based Binder Enabling Strong Polysulfide Anchoring for High-Energy Lithium-Sulfur Batteries

Journal:	*Journal of Materials Chemistry A*
Manuscript ID	TA-ART-11-2018-011384.R1
Article Type:	Paper
Date Submitted by the Author:	20-Dec-2018
Complete List of Authors:	Fu, Xuewei; Washington State University, School of Mechanical and Materials Engineering Scudiero, Louis; Washington State University, Chemistry Zhong, Katie; Washington State University, Mechanical and Materials Engineering

A Robust and Ion-Conductive Protein-Based Binder Enabling Strong Polysulfide Anchoring for High-Energy Lithium-Sulfur Batteries

Xuewei Fu[1], Louis Scudiero[2] and Wei-Hong Zhong[1]*

1. School of Mechanical and Materials Engineering, Washington State University, Pullman, WA 99164, USA.

2. Department of Chemistry, Washington State University, Pullman, WA 99164, USA.

Corresponding Author

* katie_zhong@wsu.edu (W.-H. Zhong)

Abstract

Due to the large volume change of sulfur and diffusion of dissolved polysulfides, developing high-performance binder with functions beyond mechanical adhesion/support for sulfur cathode is in high demand. This is especially true for the success of high-loading sulfur cathode. Here, we report a soy-protein-based binder with high mechanical robustness and multiple functions for high-energy lithium-sulfur batteries. The multi-functional binder (denoted as SP-PAA) is fabricated via facilely incorporating soy protein (SP) with poly(acrylic acid) (PAA) and has been demonstrated to effectively buffer the large volume change of the sulfur cathode during cycling. More significantly, the abundant polar groups (e.g. amine, carboxyl groups, etc.) of soy protein empower the binder with strong capability of adsorbing polysulfides, as evidenced by density functional theory (DFT) calculations. Meanwhile, the good ion-conduction ability of soy protein notably promotes the electrochemical reactions. With the use of this binder, the electrochemical performances (e.g. capacity, cycle stability and rate capability) of the sulfur cathode are substantially enhanced. In addition, owing to the excellent mechanical properties of SP-PAA and its effects on improving electrode microstructures, high-loading sulfur cathodes (> 5 mg/cm^2) with good and stable performances are achieved . The performances are also attributed to the roles that SP-PAA plays in adsorbing polysulfides, sustaining structural stability and promoting electrochemical reactions. This study brings about a cost-effective strategy for fabrication of superior binder by exploiting natural materials and leads to realization of high-loading sulfur cathodes for mass production.

Keywords: multi-functional binder, ion-conduction, soy protein, polysulfide-anchoring, high-loading sulfur cathode

Graphic abstract

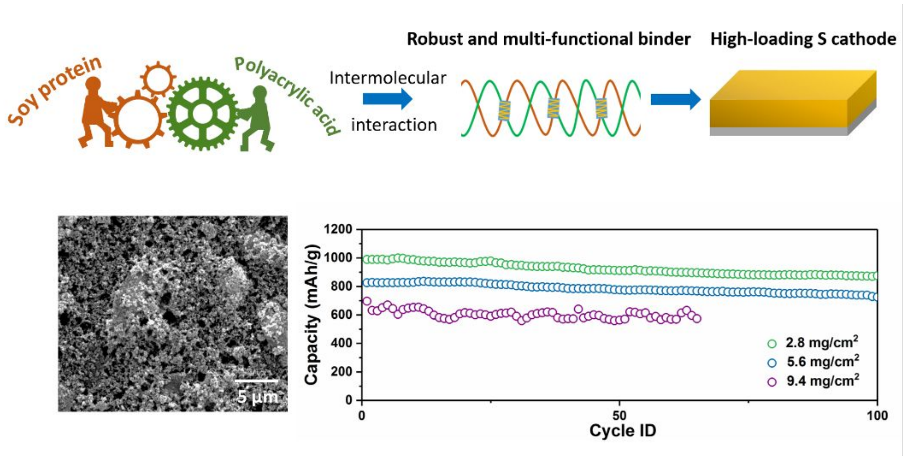

A table of contents entry: A protein-based robust binder was developed to strongly adsorb polysulfides and buffer large volume change for high-loading sulfur cathodes.

1. Introduction

Lithium-ion batteries with high energy-density and capacity have continuously dominated the energy storage market in multiple industry sectors such as electric vehicles, portable electronics, large-scale power supply systems. Among various rechargeable battery systems, lithium-sulfur (Li-S) batteries have received ever-increasing attention due to their superior advantages in specific capacity (1675 mAh/g)[1] and energy density (2600 Wh/kg)[2], which are five times higher than that of conventional lithium-ion batteries based on intercalation compound cathodes (e.g. $LiFePO_4$, $LiCoO_2$, $LiMn_2O_4$).[3,4] However, before the practical use of Li-S batteries, several critical challenges need to be overcome, which mainly originate from: (1) insulating nature of S and polysulfides, which limits the electronic transport inside the S cathode bulk; (2) dissolution and diffusion of polysulfides leading to shuttling effect, which consumes active materials and reduces capacity; (3) large volume change of S during cycling (~ 80%) that disrupts the integrity and structural stability of S cathode.[5–7] Aiming to address these issues, considerable efforts have been focused on constructing advanced composite S cathodes, which mainly involves encapsulating S into a carbon host such as hollow carbon spheres[8–10], porous carbon[11–13], graphene[14–16], carbon nanotubes[17–19], carbon nanofibers[20–23], or their heteroatom-doped derivatives[24–28]. These attempts have made substantial progress on solving some aspects of the problems and pushed forward the engineering of Li-S batteries. However, the critical shortcomings of these strategies are involving complicated and costly fabrication processes and usually applicable to low loading level of the active materials, making them not appropriate for broad practical applications.

Despite of its low loading percentage (usually < 10 wt%) in an electrode, binder is a crucial component binding active materials and conductive fillers together to form conductive networks around active materials and glue them with the current collector. At the same time, binder is essential for controlling the overall microstructures (e.g. porous structure, interfaces and conduction networks), mechanical properties and structural integrity of an electrode.[29,30] In particular, for high-capacity electrodes such as S cathode, binder plays a critical role in maintaining the structural integrity and stability of the S cathode, which can be significantly damaged by large volume change of S and dissolution of the intermediates (polysulfides) during lithiation/de-lithiation process.[31,32] Thus, a mechanically strong binder is highly desired by advanced S cathodes. More importantly, the easy dissolution and diffusion of polysulfides in an organic liquid electrolyte calls for additional functions of the binder beyond mechanical robustness, such as adsorbing the polysulfides, in order to confine the active materials within the cathode region to alleviate the shuttling effect. Therefore, rationally designing a suitable binder is of great significance for enhancing the properties of S cathodes. A traditional binder such as poly(vinylidene fluoride) (PVDF) acts as a simple “physical adhesive” enabling mechanical connection between S active materials and conductive fillers, but it lacks the capability of binding polysulfides, despite of its excellent mechanical/electrochemical stability. In this regard, tremendous endeavors have been devoted to developing various advanced robust and functional binder materials.

Over the past few decades, polar polymers have been extensively studied as they can offer strong adsorption of polysulfides via dipolar interactions.[33–35] For example, Liu et al.[36] demonstrated a cross-linked network binder of sodium alginate-Cu with strong chemical binding effects with polysulfides and good mechanical properties to significantly improve the electrochemical performance of the resulting S cathode. Another example was reported by Chen et al.[4] who developed a hydrophilic functional binder of PPA, which was able to strongly anchor polysulfides and presented excellent mechanical properties resulting in a high-loading S cathode. In addition to polar polymers, recently ionic polymers have emerged as one type of promising binder materials that can provide electrostatic interactions with polysulfides.[37] Namely, a type of polycation binder (PDAT) reported by Su et al.[38] was demonstrated to possess very strong interactions with polysulfides due to its positively charged backbone and the polysulfide anions. Zeng et al.[39] revealed a multi-dimensional polycation β-cyclodextrin (β-CDp-N^+) binder, in which the cations could help immobilize polysulfides, and the hyperbranched network structure could accommodate the volume change. In addition to abovementioned binder materials with improved mechanical properties and adsorption of polysulfides, some other unique binders endowed with additional functions have been of great interest. For example, PEDOT:PSS-Mg^{2+}[40], PEB[41], comb-like PSPEG[42], etc., which themselves possess electrical or ionic conductivity, have been reported to make great contributions to the electrochemical performances. In a nutshell, developing multi-functional binder materials with superior mechanical properties is in critical need by advanced high-performance S cathodes, which is extremely important for scalable production.

Because of these considerations, in this work we design and fabricate a new multi-functional binder based on soy protein (SP) incorporated with poly(acrylic acid) (PAA), which integrates high mechanical strength, strong polysulfide anchoring and good ion-conduction capability. The synergistic effects and intermolecular interactions between the two materials result in a robust and multi-functional network binder. With the use of this multi-functional binder, an advanced S cathode with improved microstructures, robust and porous conduction networks facilitating good ion-conduction, and excellent confinement of polysulfides is achieved. As a result, the mechanical properties and electrochemical performances (e.g. specific capacity, cycle stability, C-rate performance) of the S cathode are significantly improved. Furthermore, we surprisingly find that good and stable performances can be realized on high-loading S cathodes (above 5 mg/cm^2 loading of S), which deliver comparative areal capacities with commercialized lithium-ion batteries. The roles that the multi-functional binder play in the improvements of the properties/performances of the S cathodes are systematically analyzed and verified by density functional theory (DFT) calculations.

2. Materials and methods

2.1. Preparation of SP-PAA network binder

SP powders (donated by Archer Daniels Midland) were first denatured in an acetic acid solution with a pH value of 2 at 95 °C under stirring for 1 h. The denaturation process was able to significantly reduce the particle size of SP to nanoscale.[43] The solid concentration of the solution was 3 wt%. Then the SP solution was cooled down to room temperature naturally for subsequent experiment. At the same time, a PAA solution with a concentration of 3 wt% was prepared by dissolving PAA powders (Mw = 450,000 g/mol, Sigma Aldrich) in the acetic acid solution (pH = 2) under stirring until completely dissolved. Afterward the above two solutions were mixed together according to a weight ratio of SP : PAA = 3 : 2 and stirred for 1 h at room temperature. In this mixing process, the formation of hydrogen bonding occurred to generate SP-PAA network binder. The prepared mixture solution of SP-PAA was used as the binder for subsequent experiments.

2.2. Fabrication of S cathode with various binders and cell assembly

Three types of binder solutions: SP, PAA and SP-PAA, with a solid concentration of 3 wt% were used to fabricate S cathodes. Briefly, the S cathodes were prepared by mixing 67.5 wt% S particles

(Sigma Aldrich), 22.5 wt% carbon black (SuperC45, MTI) and 10 wt% binder in a mortar and the mixture was milled for 15 min to form homogeneous slurry. The slurry was casted onto a carbon-coated aluminum foil by a doctor blade controlling the thickness and was dried at room temperature for 1 h. The obtained electrode laminates were punched into 0.5-inch circular disks with various S loadings and were further dried in a vacuum oven for 12 h to completely remove the residual solvents and moisture prior to being transferred to the argon-filled glove box. 2032-type coin cells were assembled with the Celgard (PP/PE/PP, trilayer) separator by using a liquid electrolyte solution composed of 1 M LiTFSI dissolved in mixed solvents of DOL/DME (1 : 1 by volume) with 2 wt% $LiNO_3$ as additive. The electrolyte/sulfur ratio was kept constant to be 10 μL/mg.

2.3. Preparation of Li_2S_6 solution and visualized adsorption testing

To prepare Li_2S_6 solution (0.05 mM), a certain amount of Li_2S powders (Sigma Aldrich) and S powders were added into the mixed solvent of DOL/DME (1 : 1 by volume) according to a molar ratio of 1 : 5. The mixture was vigorously stirred at 50 °C for 3 h in the argon-filled glove box to finally obtain the Li_2S_6 solution. To demonstrate the adsorption ability of various binders, composites of binder/CB were first prepared with a mass ratio of 1 : 1. Various binder solution and CB particles were mixed in a mortar uniformly and dried at room temperature. The composites were further dried in a vacuum oven for removing residual solvents and moisture and were transferred into the argon-filled glove box. For the visualized adsorption testing, 0.1 g composites were added into 10 mL Li_2S_6 solution in the glove box.

2.4. Density functional theory (DFT) calculation

The molecular simulations were carried out at the B3LYP 6-31+G(d,p) level of DFT using Gaussian 5.0, based on the previous study[44]. The geometries of the molecules were first optimized to the minimum energy. For SP simulations, multiple amino acid sequences were randomly picked according to the PDB file (ID: 1UIK). For each amino acid sequence, at least three different types of amino acids were included to finally cover 18 kinds of amino acids of SP in total. The adsorption binding energy (Ea) was computed to inspect the binding energy of Li_2S with N and O atoms in the segments of PAA and various amino acids. It is assumed that only one N or O atom interact with Li ion of Li_2S. Ea can be determined via equation (3):

$$Ea = E_{Li_2S} + E_{polymer} - E_{Li_2S + polymer} \tag{3}$$

where E_{Li_2S}, $E_{polymer}$, and $E_{Li_2S+polymer}$ refer to the minimized ground-state energies of Li_2S, polymer and the complex of Li_2S and polymer, respectively.

2.5. Material characterizations

Characterizations of binder. Infrared spectra of the solid binder films were recorded by a Fourier transform infrared spectrophotometer (FTIR) (Nicolet iS10) using ATR mode. The viscosity of the various binder solutions (5 wt%) was measured by a viscometer (Brookfield) and the tip rotation speed was kept constant to be 10 RPM. Dynamic mechanical analysis (DMA) was used to examine the storage modulus of the solid binder films in frequency-strain mode at 1 Hz. The liquid electrolyte uptake of the binder films was measured by immersing the films in a liquid electrolyte solution and weighing the mass of the films at varying time intervals. When taking the films out for weighing, the residual liquid electrolyte was carefully wiped away by Kimwipes tissue. The liquid electrolyte uptake was determined via equation (4):

$$\eta = \frac{m_a - m_o}{m_o} \times 100 \tag{4}$$

Where η (%) refers to the liquid electrolyte uptake; m_o and m_a refer to the mass of the film before and after immersing in the liquid electrolyte, respectively.

Characterizations of electrode. The morphology of the free surfaces of electrodes was investigated by scanning electron microscopy (SEM, Quanta 200F). The mechanical properties of the electrodes were tested by a rheometer (HR-2, TA Instruments) via indentation and stress-relaxation. In a typical measurement, the electrodes before and after immersing in a liquid electrolyte for 5 min were attached onto the sample holder. Meanwhile, a steel tip (diameter: 8 mm) kept approaching toward the electrodes with a constant speed of 1 μm/s until reaching a maximum axial force of 25 N. Then the tip stopped moving and stayed static for 2 min. The variation of axial force in the whole process was recorded with time. The adhesion property of the electrodes was investigated by a peel-off testing carried out using the same rheometer. The electrodes were first tightly attached on the sample stage by a double-sided tape. Then a 3M tape was adhered to the electrode surface, with an effective contact area of 1.5 cm^2 (1 cm x 1.5 cm), while the other side of the 3M tape was tightly fixed to the steel tip. The steel tip with the tape kept moving upward with a constant speed of 300 μm/s. The evolution of axial force was recorded until the electrode laminate completely detached from the current collector. The electrical conductivity of the electrodes under dynamic shearing was recorded by a SourceMeter (Keithley 2410). The setup is shown in **Figure 4e**. The dynamic shearing was generated by a rheometer that can precisely control the frequency and strain amplitude to produce various deformation intensities (see the inset table in **Figure 4f**). The SourceMeter was connected with the rheometer, recording the evolution of electrical conductivity with various deformation rates. The electrical conductivity was obtained via $\sigma = l/RA$, where l is the thickness of the electrode; R is the resistance determined by the SourceMeter; A is the effective area of the electrode contacting with the tip (50.24 mm^2).

Electrochemical characterizations. The charging/discharging curves, cycle stability and C-rate performance of the Li-S cells were obtained via cycling the cells with a cut-off voltage of 1.5 – 2.8 V by using a battery analyzer (BST8-MA, MTI) at room temperature. Electrochemical impedance spectroscopy (EIS) was used to measure the impedance spectra of the Li-S cells by an electrochemical workstation (CHI 660E) in a frequency range of 0.01 - 1 M Hz. The open-circuit voltage of the Li-S cells was measured by using an electrochemical workstation via the Open Circuit Potential mode at various time intervals.

3. Results and discussion

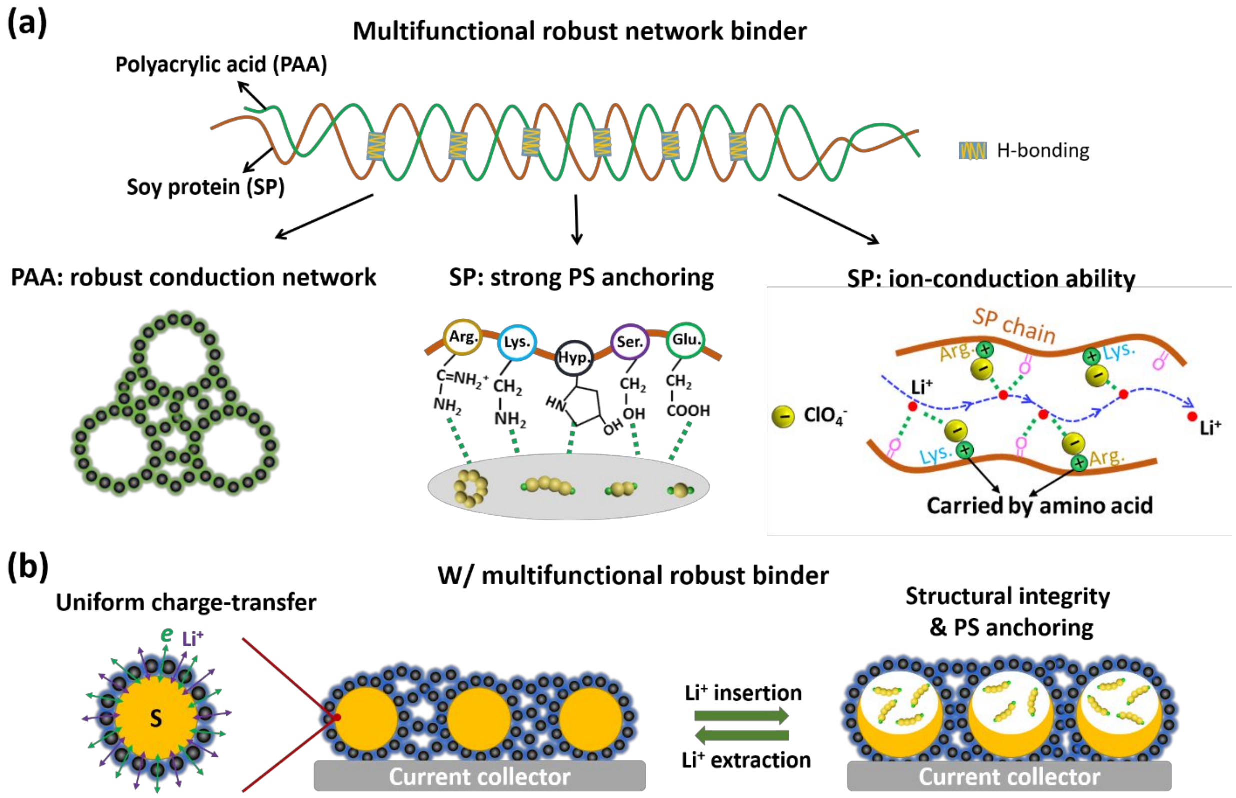

Figure 1. Schematic illustration of the design strategy of the robust and multi-functional binder (SP-PAA) via incorporating two functional materials. (a) Illustration of the design concept for fabricating the multi-functional robust binder by taking advantage of two functional

materials. (b) Schematic of the structural changes of S cathodes with a multi-functional robust binder during lithiation/de-lithiation process. Note: PS refers to polysulfide.

Binder is a critical ingredient for controlling the overall electrode structures in batteries. In particular, for S cathodes that experience a dramatic volume change and dissolution of S active materials, the binder becomes the only “soft” material that can buffer the deformation and help to stabilize the electrode structures. Traditional binders such as PVDF, in spite of their acceptable adhesion and good electrochemical stability, are insufficient for both accommodating the large volume change and preventing the diffusion of polysulfides, due to the nonfunctionalized chain structures. Consequently, the microstructures of the S cathode will be greatly destroyed and meanwhile, the shuttling effect will still occur. Therefore, building robust conduction networks with good ability of anchoring polysulfides around S active materials is believed to be an effective strategy to stabilizing S cathodes. This is realized by applying a multi-functional robust binder demonstrated in this work. As depicted in **Figure 1a**, we design a new multi-functional robust binder by capitalizing the merits of two materials: soy protein (SP) and poly(acrylic acid) (PAA). As is well known that a number of polar groups (e.g. amine, carboxyl, carbonyl groups, etc.)[45] has been proved to possess strong binding effect with polysulfides due to dipolar interactions. SP as a natural protein, possesses 18 different kinds of amino acids (see the amino acid profile in **Table S1**)[46], making it rich in various polar functional groups. The abundant functional groups of SP enable it to strongly adsorb polysulfides with mitigating the irreversible dissolution of polysulfides. Also, SP presents a good ionic conductivity (ca. 10^{-5} S/cm, 25 °C) as revealed by our previous study[47], which can promote the transport of Li^+ in the S cathode bulk to significantly boost the electrochemical reactions especially at high current densities. This is because the oxygen atoms in the protein backbone and the negatively charged amino acids (Arg. and Lys.) that attract anions (e.g. ClO$_4^-$) perform as coordination sites, enabling fast hopping of Li$^+$ among them. At the same time, PAA is a widely-used aqueous binder material that possesses certain ability of binding polysulfides[32,48]. In addition to this property, we explore that PAA presents superior mechanical properties and is conducive to form stable interfaces between S active materials and conductive fillers, thus resulting in robust conduction networks around S particles. Due to the strong interactions between SP and PAA, a multi-functional network binder is fabricated with integration of strong polysulfide anchoring, robust mechanical properties and good conduction of Li$^+$, which tremendously enhances the mechanical properties and electrochemical performances of the S cathode as illustrated in **Figure 1b**. The synergy of the multi-functional binder will make great contribution to the transport of ions/electrons, structural stability of S cathode and adsorption of polysulfides.

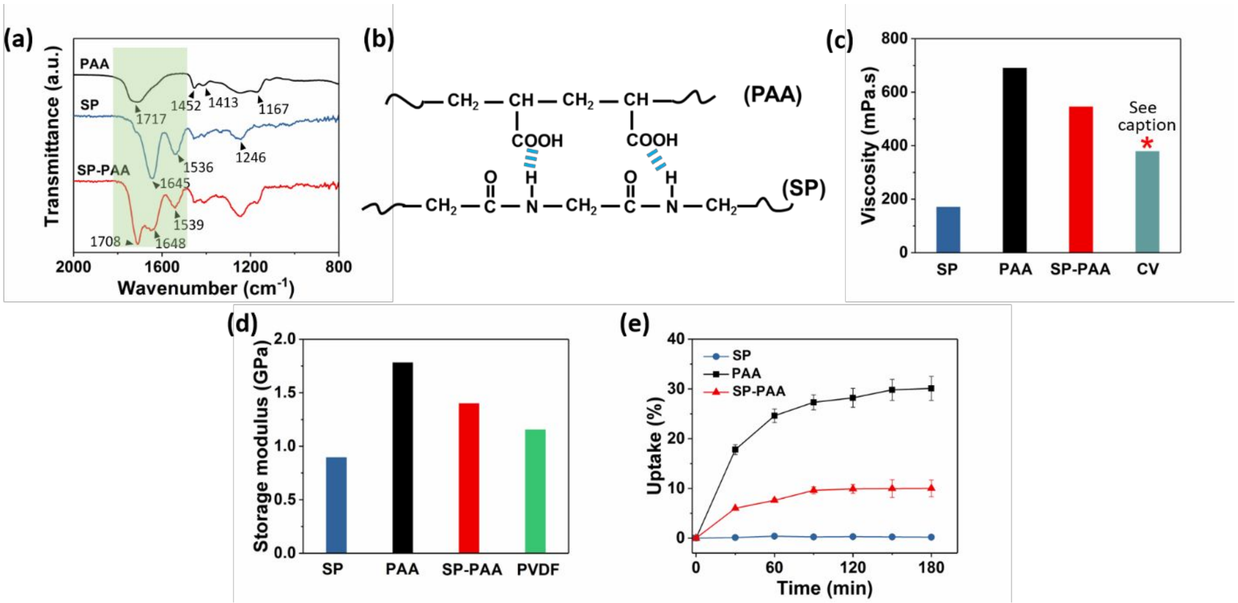

Figure 2. Properties of the multi-functional robust binder: SP-PAA. (a) FTIR spectra of SP, PAA and SP-PAA. (b) Schematic of the formation of hydrogen bonding between PAA and SP. (c) Viscosity of SP, PAA and SP-PAA solutions (5 wt%) at 25 °C. Calculative viscosity (CV) is

calculated based on the mass ratio of SP and PAA in SP-PAA (3 : 2). (d) Storage modulus of SP, PAA and SP-PAA solid films obtained by DMA tensile mode at 25 °C. (e) Liquid electrolyte uptake of SP, PAA and SP-PAA solid films at 25 °C.

As shown in **Figure 2a**, the Fourier-transform infrared spectroscopy (FTIR) was performed to investigate the interactions between SP and PAA. It can be found that the FTIR spectrum of PAA reveals several characteristic peaks at 1167, 1413, 1452 and 1717 cm^{-1} attributed to C-O stretching, C-O-H in-plane bonding, $-CH_2$ stretching and C=O stretching, respectively.[49,50] SP shows multiple dominant peaks at 1246, 1536 and 1645 cm^{-1}, which can be assigned to C-N stretching (amide III), N-H bending (amide II) and C=O stretching (amide I), respectively.[51,52] Regarding their combination, SP-PAA, it can be seen that the FTIR spectrum displays the characteristic peaks of SP and PAA, indicating the existence of both materials. In particular, one finds notable peak shift for SP-PAA. Specifically, the peaks originally at 1536, 1645 and 1717 cm^{-1} respectively corresponding to N-H bending (amide II), C=O stretching (amide I) and C=O stretching obviously move to 1539, 1645 and 1708 cm^{-1} after incorporation of SP and PAA. This indicates that there is a very strong intermolecular interaction between -NH group of SP and -COOH group of PAA via forming hydrogen bonding as shown in **Figure 2b**. The strong intermolecular interaction eventually results in the formation of network structure by SP and PAA, contributing greatly to the mechanical properties of the resulting SP-PAA binder. In addition, as shown in **Figure 2c** the viscosity of the SP-PAA solution (545 mPa.s) is remarkably higher than the calculative viscosity (CV) (378 mPa.s) determined by the mass ratio of SP and PAA in SP-PAA (3 : 2), which also proves the intermolecular binding effect between SP and PAA.[53]

The mechanical properties of the binder play an important role in buffering the volume deformation that the S cathode will experience over alloying/de-alloying process with Li. We measured the storage modulus of the various solid binder films by dynamic mechanical analysis (DMA) to be compared with PVDF film. As displayed in **Figure 2d**, of the four types of binder films, PAA presents the highest modulus of 1.78 GPa that is about twice that of SP (0.91 GPa). At the same time, SP-PAA reveals a modulus of 1.39 GPa, only slightly lowered by SP, which is also higher than that of PVDF with a modulus of 1.15 GPa. The high modulus of SP-PAA is significantly contributed by the robust network structure derived from the strong intermolecular interactions between SP and PAA. Further, for actual battery applications, the liquid electrolyte uptake of the binder is another critical factor considerably affecting the electrode structures and electrochemical performances of the batteries. An appropriate uptake level of liquid electrolyte will be beneficial for maintaining the structural stability and integrity of the electrodes and constructing fast ion-transport pathways inside the electrodes simultaneously. We inspected the liquid electrolyte uptake of the SP, PAA and SP-PAA solid films by immersing them in the electrolyte solution (1 M LiTFSI dissolved in DOL/DME (1 : 1 by volume)) and calculating the weight gain over specific time intervals. The results are displayed in **Figure 2e**. It is found that SP is not able to adsorb any liquid electrolyte over all timeframe, showing negligible liquid electrolyte uptake. On the contrary, PAA can remarkably uptake more liquid electrolyte (ca. 30%), while SP-PAA presents a medium electrolyte uptake of ca. 9%. The aforementioned results indicate that two points are worthy of discussion here. Firstly, the trifling electrolyte uptake of SP helps to maintain the mechanical properties of SP and thereby the structural stability of the S cathodes in batteries; however, on the other hand, it impedes the permeation of liquid electrolyte and the construction of ion-conduction pathways around the S particles. Secondly, although PAA shows high electrolyte uptake level, which benefits the ion-conduction inside the S cathodes, the mechanical properties of the PAA binder itself and the resulting S cathodes will be sacrificed accordingly. Thus, the combination of SP and PAA may result in a proper electrolyte uptake level that assists in maintaining a good balance between mechanical properties and ion-conduction capability, which will be discussed in detail later.

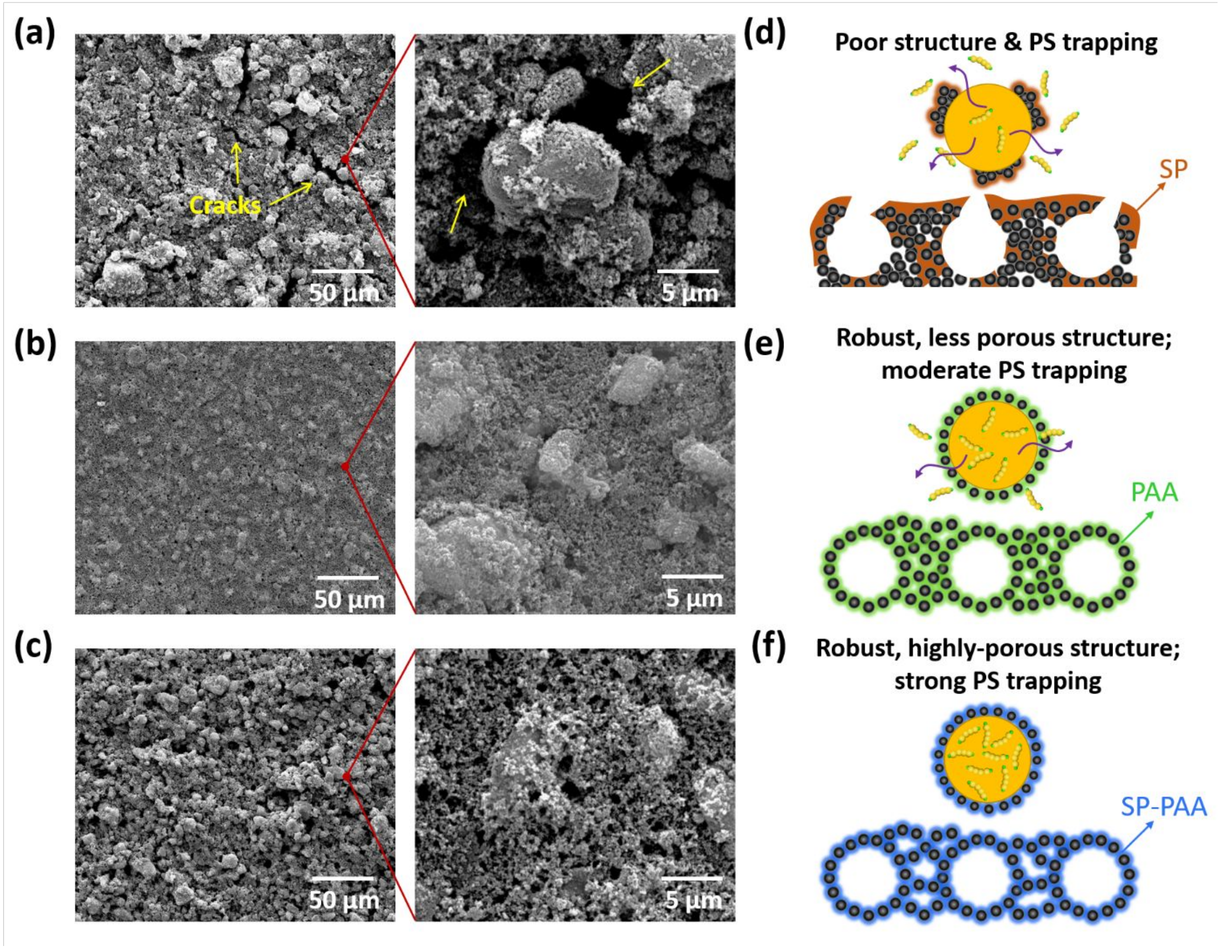

Figure 3. Microstructures of S cathodes with different binders. (a) – (c) SEM images of the S cathodes with SP, PAA and SP-PAA as the binder, respectively. (d) – (f) Illustration of the structures of the S cathodes prepared with SP, PAA and SP-PAA, respectively.

As illustrated in **Figure 1b**, a robust and multi-functional binder that can form strong and functional conduction networks around S particles is of great interest to the stabilization of the S cathodes and alleviation of the diffusion of polysulfides out of the S cathodes. We surprisingly find that the SP-PAA binder effectively improves the electrode microstructures such as uniformity, porous structure and interfaces. In specific, for the S cathode with SP, the SEM images in **Figure 3a** show many cracks on the electrode surface indicating a very poor structural integrity. In addition, one finds that the conduction networks around S particles are very weak with poor interfaces and even big cracks between S particles and conductive fillers (carbon black, CB). In contrast, PAA is found to effectively improve the structural properties of the S cathode. As shown in **Figure 3b**, the microstructure of the S cathode dramatically changes as compared with the case of SP. It can be seen that the electrode presents a very uniform overall microstructure and no noticeable cracks can be observed. Taking a closer look, the CB particles are well distributed around S particles, forming much improved interface quality between them. Moreover, it is revealed that the composite of CB and PAA in the S cathode leads to a relatively compact porous structure with good uniformity and contact with S particles, generating stable conduction networks around S particles. In the case of SP-PAA shown in **Figure 3c**, one can observe that the accumulation of CB particles is much looser than that of PAA electrode yielding more big pores on the electrode surface with a generally uniform structure, which significantly helps the permeation of liquid electrolyte. Meanwhile, the CB particles encompass around the S particles generating stable interfaces and highly-porous and robust conduction networks.

The structural properties of the S cathodes as discussed above, including uniformity, porous structure and interfaces, tremendously impact the charge-transport, structural stability of the electrodes and absorption of polysulfides in charging/discharging process. For the S cathode prepared with SP as illustrated in **Figure 3d**, even though SP shows strong polysulfide adsorption capability that will be discussed in detail later, its poor structural integrity with numerous cracks and weak interfaces between S particles and CB results in very unstable structures of the S cathode when experiencing notable volume change during cycling. As a result, the overall integrity of the electrode and the conduction networks for ions/electrons are ruined; meanwhile, the polysulfides still diffuse out of the S cathode eventually. In contrast, PAA and SP-PAA can remarkably improve the structural factors, and thus the mechanical/electrochemical properties of the S cathodes. As demonstrated above, PAA helps form uniform electrode structures and robust conduction networks around S particles. Such improved microstructures benefit the mechanical and structural stability of the S cathode. In addition, the robust conduction networks built from PAA/CB assist in binding the dissolved polysulfides due to some interaction between PAA and polysulfides as reported previously[48] (see **Figure 3e**). Nonetheless, the less porous structure of the electrode may impede the permeation of liquid electrolyte to the electrode bulk. As further improvement, SP-PAA does not only give rise to uniform electrode structures (e.g. stable interface, good porous structure, etc.) contributing to mechanical properties and charge-transfer of the electrode, but also strong capability of binding polysulfides. Such strong binding capability is enabled by the various functional groups of SP (to be demonstrated in detail later) and advanced porous conduction networks that maximize the function of SP-PAA for adsorbing polysulfides.

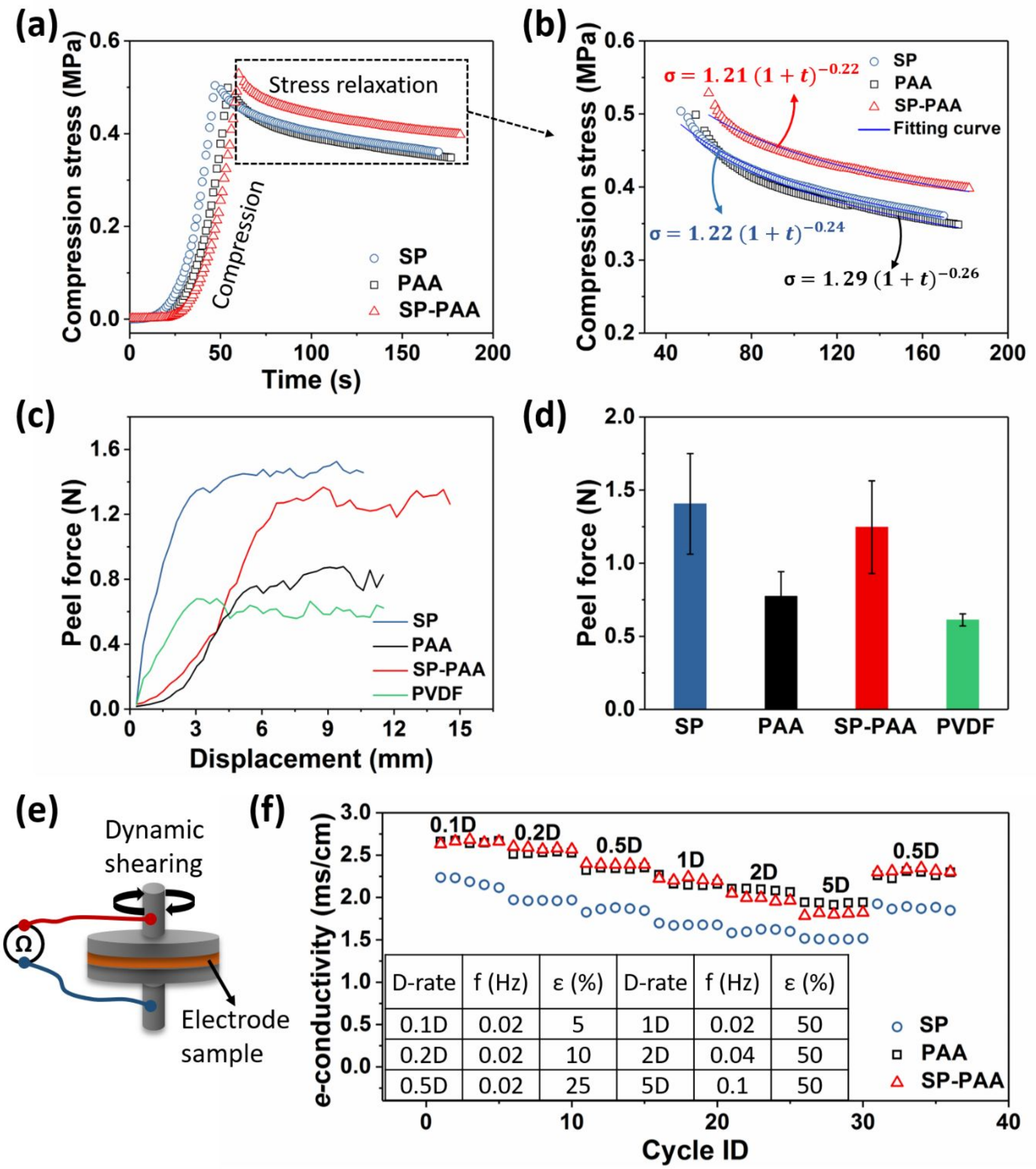

D-rate	f (Hz)	ε (%)	D-rate	f (Hz)	ε (%)
0.1D	0.02	5	1D	0.02	50
0.2D	0.02	10	2D	0.04	50
0.5D	0.02	25	5D	0.1	50

Figure 4. Mechanical properties, adhesion property and electrical conductivity stability of S cathodes with different binders. (a) – (b) The evolution of compression stress versus indentation time for wet S cathodes with different binders, measured by compression and stress-relaxation. Prior to testing, the electrodes were soaked in liquid electrolyte solution for 5 min. (c) Peel force versus displacement for the S cathodes with different binders by peel-off testing. (d) Comparison

of peel off force for S cathodes with different binders. (e) Illustration of the setup for measuring the electrical conductivity of S cathodes affected by dynamic shearing. (f) The effects of dynamic shearing on the electrical conductivity of the S cathodes with different binders at varying D-rates (the inset table shows the specific parameters for adjusting the D-rate).

It is well established that the mechanical properties of electrodes, especially high-capacity electrodes such as S cathode, are extremely important for device applications. The huge compression force from cell packing and the large volume change in electrochemical reactions are both critical inducements for structural instability of the S cathodes. Therefore, good mechanical properties and structural stability are imperative for advanced S cathodes that are a result of comprehensive contributions from the electrode microstructure factors (e.g. uniformity, porous structure, interfaces, etc.). We have demonstrated that the microstructures of the S cathodes are significantly impacted by the various types of binders, and PAA and SP-PAA result in much uniform electrode structures. To elaborate the advantages of the specific binders, we further investigated the mechanical properties of the S cathodes before and after immersing in liquid electrolyte via rheological measurement. As shown in **Figure 4a**, the measurement includes two stages: compression and stress-relaxation. In the first stage, compression stage, a metal tip with a diameter of 8 μm continuously approaches he electrode at a constant moving speed of 1 μm/s. In this process, the compression stress steeply grows with the compression strain until reaching an axial force of 25 N. Afterward, the tip stops moving and keeps a constant compression strain, and in this stress-relaxation stage, the compression stress gradually decays with time. The stress-relaxation stage can reveal how stable the electrode is after undergoing indentation and a certain compression strain, which is a reflection of mechanical and structural stability of the electrode. More detailed information about the testing can be found in Experimental section.

Figure S1 shows the evolution of compression stress with time in stress-relaxation process for the dry S cathodes with different binders. The decay behavior of the compression stress can be well-fitted via equation (1):

$$\sigma = m\,(1+t)^n \tag{1}$$

where σ is the compression stress and t is the time. Constants m and n are relevant to the decay rate of the compression stress. It is believed that the faster the decay rate, the poorer the structural stability. It can be seen in **Figure S1** that the S cathode with PAA shows the slowest decay rate of compression stress, with the smallest absolute values of m and n: 0.62, 0.04, respectively. However, SP is found to exhibit the fasted decay rate revealed by the largest absolute values of m (0.64) and n (0.06). SP-PAA presents a medium decay rate (absolute values of m and n are 0.63 and 0.05, respectively). The results are in good agreement with the morphological studies and the moduli of the binders as discussed above. For example, PAA possesses the highest modulus (1.78 GPa) and PAA electrode shows very uniform microstructures and stable interfaces, all of which are responsible for the best mechanical properties of dry PPA electrode.

Moreover, the mechanical properties of the S cathodes after immersing in the liquid electrolyte for 5 min were also examined, in order to simulate the actual conditions in batteries. As shown in **Figure 4b**, wetting of the liquid electrolyte deteriorates the mechanical properties of all electrodes, which is verified by the substantially increasing absolute values of both m and n. However, it is surprisingly found that SP-PAA electrode outperforms the PAA electrode in wet-state and delivers the best mechanical properties, which presents the smallest absolute values of m and n (1.21 and

0.22, respectively). In addition, the PAA electrode even shows much poorer mechanical properties than that of the SP electrode with much larger absolute values of *m* and *n* as compared with the SP electrode. The dramatically reduced mechanical properties of the PAA electrode after immersing in the liquid electrolyte mainly result from the notable swelling of PAA in the liquid electrolyte as revealed in **Figure 2d.** In a nutshell, SP-PAA makes great contributions to the mechanical properties of the electrode from two aspects. Firstly, the use of SP-PAA results in robust electrode microstructures with good uniformity, porous structures and good interaction on interfaces. These structural features effectively reinforce the mechanical and structural stability of the S cathode. Secondly, SP-PAA presents an appropriate swelling property in liquid electrolyte, which assists in maintaining the overall structural characteristics and mechanical properties of the S cathode after wetting by the liquid electrolyte.

In addition to mechanical properties, strong adhesion of the electrode laminate to the current collector is critically required for realizing stable and high-performance batteries. In this work, the adhesion property of the electrodes was studied by peel-off testing using a 3M tape. The peel forces against displacement for various S cathodes are shown in **Figure 4c** and the obtained peel forces are summarized in **Figure 4d** in comparison with the S cathode with the PVDF binder. It clearly reveals that the peel force of SP electrode is the highest (ca. 1.5 N), and PVDF electrode renders the lowest peel force of only ca. 0.6 N. The peel force of the SP-PAA electrode is found to be a little lower than that of the SP electrode, which is ca. 1.3 N. The abovementioned results indicate that SP provides very strong adhesion to the current collector, which should be attributed to its abundant functional groups including polar/nonpolar and charged groups. The various kinds of functional groups bring about rich interactions with the current collector, i.e. Van der Waals force, charge-charge interaction, etc., to effectively reinforce the adhesion between the electrode and the current collector.[54,55] Thus, the existence of SP in SP-PAA can significantly improve the adhesion property of the SP-PAA electrode.

For high-capacity electrodes such as S cathode, construction of robust and stable conduction networks is crucial during electrochemical reactions, as the large volume change will severely impact the conduction pathways. As revealed above in morphological studies, three types of binders lead to distinctly different microstructures, i.e. uniformity/interfaces. To interpret the significance of the electrode structures in the stability of conduction networks, we measured the electrical conductivity of the electrodes while applying dynamic shearing force on the electrodes. As illustrated in **Figure 4e**, the setup includes a rheometer generating dynamic shearing on the electrode and a SourceMeter recording the electrical conductivity of the electrode. For details, please see Experimental section. Here, a series of deformation rates (D-rates) is applied via varying the parameters including frequency and strain according to equation (2):

$$D\text{-}rate = f \times \varepsilon \times 100 \tag{2}$$

where f refers to frequency and ε refers to strain. The detailed D-rates studied here are listed in the insert table in **Figure 4f.** The variation of electrical conductivity versus D-rate is also shown in **Figure 4f**. Basically, the electrical conductivity of all electrodes declines with increasing intensity of deformation due to growing breaking-down of conduction structures. In specific, the PAA and SP-PAA electrodes deliver very similar electrical conductivities with moderate deformation, e.g. ≤ 1D. When the deformation enlarges to 1D and 5D, the PAA electrode outmatches the SP-PAA electrode, due to the much better mechanical properties of the dry PAA electrode as revealed above in mechanical properties studies (**Figure S1**). In addition, owing to the poor mechanical properties and conduction network structure of the SP electrode, the electrical conductivity evidently lies in the lowest level of the three electrodes. In short, the PAA and SP-PAA electrodes present much better and more robust conduction network structures as compared with the SP electrode, which greatly stabilizes the conduction structures of the electrodes under deformation and potentially promotes the electrochemical performances of the electrodes.

To prove the effectiveness of the SP-PAA binder in improving the electrode structures, mechanical properties and thereof electrochemical performances of the S cathodes, Li-S cells with different S cathodes were assembled and tested. The S cathodes with a moderate loading of active material about 1.5 mg/cm^2 were first evaluated. The charging/discharging curves of various S cathodes measured at 0.1 A/g are displayed in **Figure 5a**. As shown, as compared with the PVDF electrode, SP, PAA and SP-PAA electrodes present remarkably higher discharge capacities. This is because PVDF fails to capture dissolved polysulfides, leading to great loss of S active materials. In specific, the SP-PAA electrode delivers the highest capacity of 1308 mAh/g, while the lowest capacity of 969 mAh/g is brought about by the PVDF electrode. Moreover, one finds that the SP-PAA electrode shows the lowest polarization with a flat discharge plateau at 2.1 V, indicating that the electrochemical reactions occur very smoothly owing to the good electrode microstructures with advanced conduction networks. Importantly, the intrinsic ionic conductivity of SP, as revealed by our previous study[47], promoting the transport of Li$^+$, also helps to facilitate the electrochemical reactions. At the same time, the PAA electrode reveals the highest polarization and the SP electrode shows a medium one. This is because the compact accumulation of CB particles with less porous structure (see **Figure 3b**) and notable swelling of PAA in liquid electrolyte as demonstrated in **Figure 2d**, greatly increases the resistance for charge-transport and deteriorates the structures of the PAA electrode as proved in **Figure 4b**. **Figure 5b** shows the voltage profiles of the SP-PAA electrode upon various cycles at 0.5 A/g. The eight voltage profiles show very good repeatability, despite of slight capacity decay with increasing cycles, which suggests that the electrochemical reactions turn out very stable and reversible during cycling.

The improvement of electrode structures significantly contributes to the electrochemical performances especially the C-rate performance. As displayed in **Figure 5c**, the capacities of the S cathode with SP-PAA are distinctly the highest of all S cathodes at all tested current densities. In specific, the capacities of SP-PAA electrode recover to ca. 1105 mAh/g when the current density decreases from 1 A/g to 0.2 A/g, which is 99.4% of the original capacities of ca. 1112 mAh/g at 0.2 A/g. The recovery ratios for SP and PAA electrodes are 98.8% and 98.9%, respectively, which are much lower than that of SP-PAA electrode. Moreover, the role of the electrode structures becomes more dominant at high current densities, as the porous conduction-network structures are essential for realizing fast charge-transport. It is specially found that at a high current density of such as 1 A/g, SP-PAA electrode still exhibits the highest capacity of ca. 686 mAh/g as compared with the electrodes with SP (ca. 578 mAh/g) and PAA (ca. 371 mAh/g). The result implies that the advantages of the enhanced structures and mechanical properties of SP-PAA electrode significantly improve the C-rate performance and enable a smooth and fast charge-transport even at high current densities.

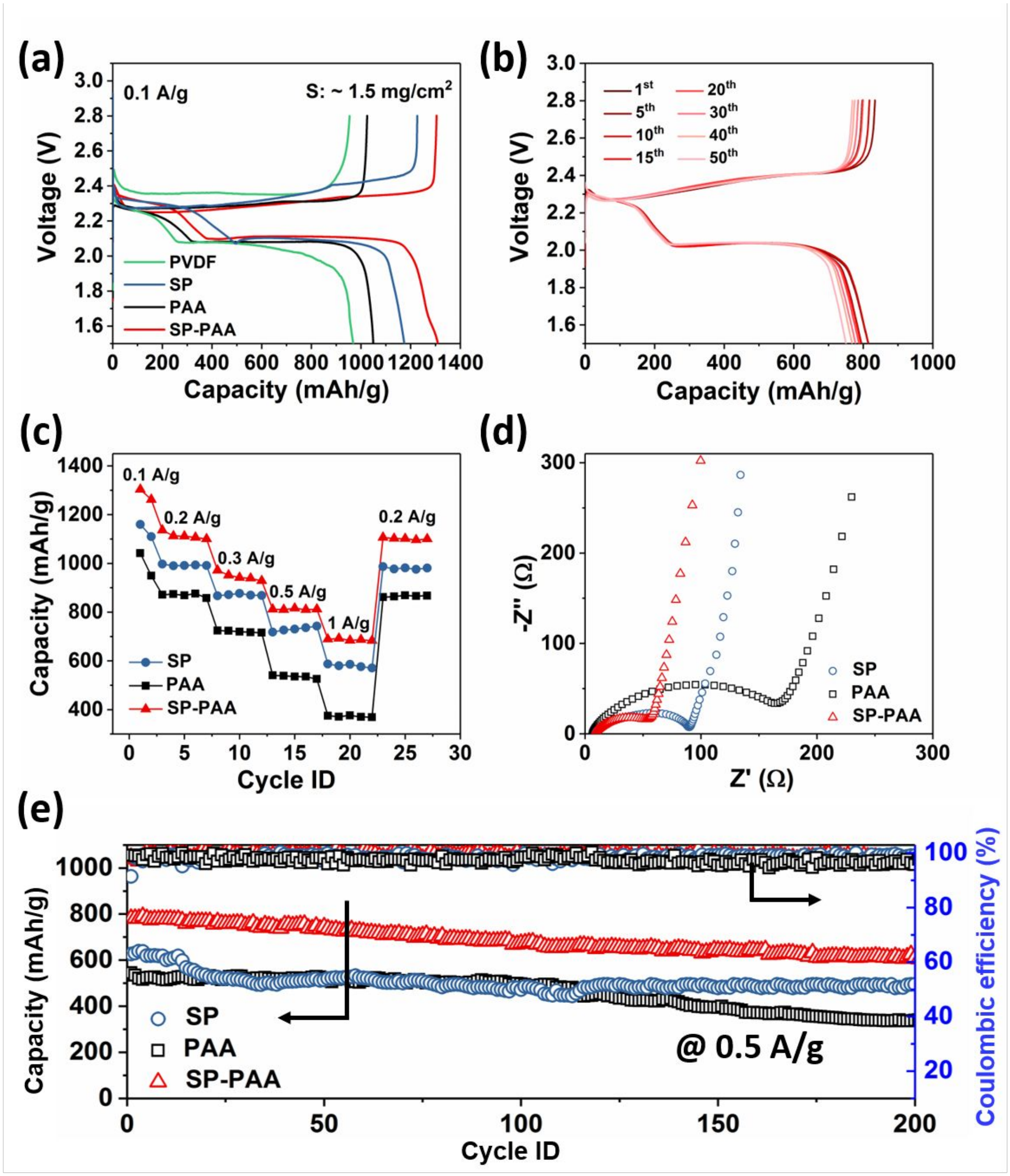

Figure 5. Electrochemical performance of the batteries with different S cathodes. (a) Voltage profiles of S cathodes with different binders at 0.1 A/g. (b) Voltage profiles of the S cathode with SP-PAA as the binder upon varying cycles at 0.5 A/g. (c) C-rate performance of S cathodes with

different binders. (d) Nyquist plot of S cathodes with different binders. (e) Cycle stability and Coulombic efficiency of S cathodes with different binders at 0.5 A/g.

The benefits of SP-PAA to the electrochemical performances were further inspected by electrochemical impedance spectroscopy (EIS). The Nyquist plot of different S cathodes is shown in **Figure 5d.** The result indicates that the SP-PAA electrode exhibits the lowest charge-transfer resistance of about 52 Ω, which can be defined as the diameter of the semi-circle in the high-frequency area arising from the interface between electrode and electrolyte.[56,57] The PAA electrode presents the highest charge-transfer resistance of ca. 172 Ω, while SP electrode reveals a much lower one (ca. 83 Ω). The lowest charge-transfer resistance of the SP-PAA electrode can be ascribed to two reasons: (1) the uniform electrode microstructure with robust porous conduction networks; (2) the good ion-conduction of SP that further facilitates the transport of Li^+. As a result, the charge-transport inside the SP-PAA electrode can be effectively promoted, which is consistent with the above electrochemical performances.

Figure 5e shows the cycle performance of the electrodes at 0.5 A/g. It is noticeably found that the SP-PAA electrode delivers the highest capacity among all electrodes. Meanwhile, the capacity of the SP-PAA electrode is very stable upon 200 cycles without evident capacity fading, presenting a high average Coulombic efficiency of 99.3%. It is also found that SP and PAA electrodes exhibit very similar capacity within about 120 cycles, although the capacity of the SP electrode apparently decays in the first couple of cycles due to the instability of the electrode by electrochemical reactions possibly. Also, an obvious capacity decay occurs on PAA electrode after about 130 cycles caused by the severe shuttling effect during cycling. The average Coulombic efficiencies of SP and PAA electrodes are determined to be 98.2 and 97.1%, respectively, which are much lower than that of the SP-PAA electrode. The above results suggest that the binder and the electrode structure play a critical role in diminishing the loss of S active materials and shuttling effect. For the SP-PAA electrode, owing to its uniform microstructure and good interfaces between S particles and CB particles, as well as the strong adsorption of polysulfides by SP-PAA, the Coulombic efficiency is substantially improved, which finally results in very stable cycling with minimized shuttling effect.

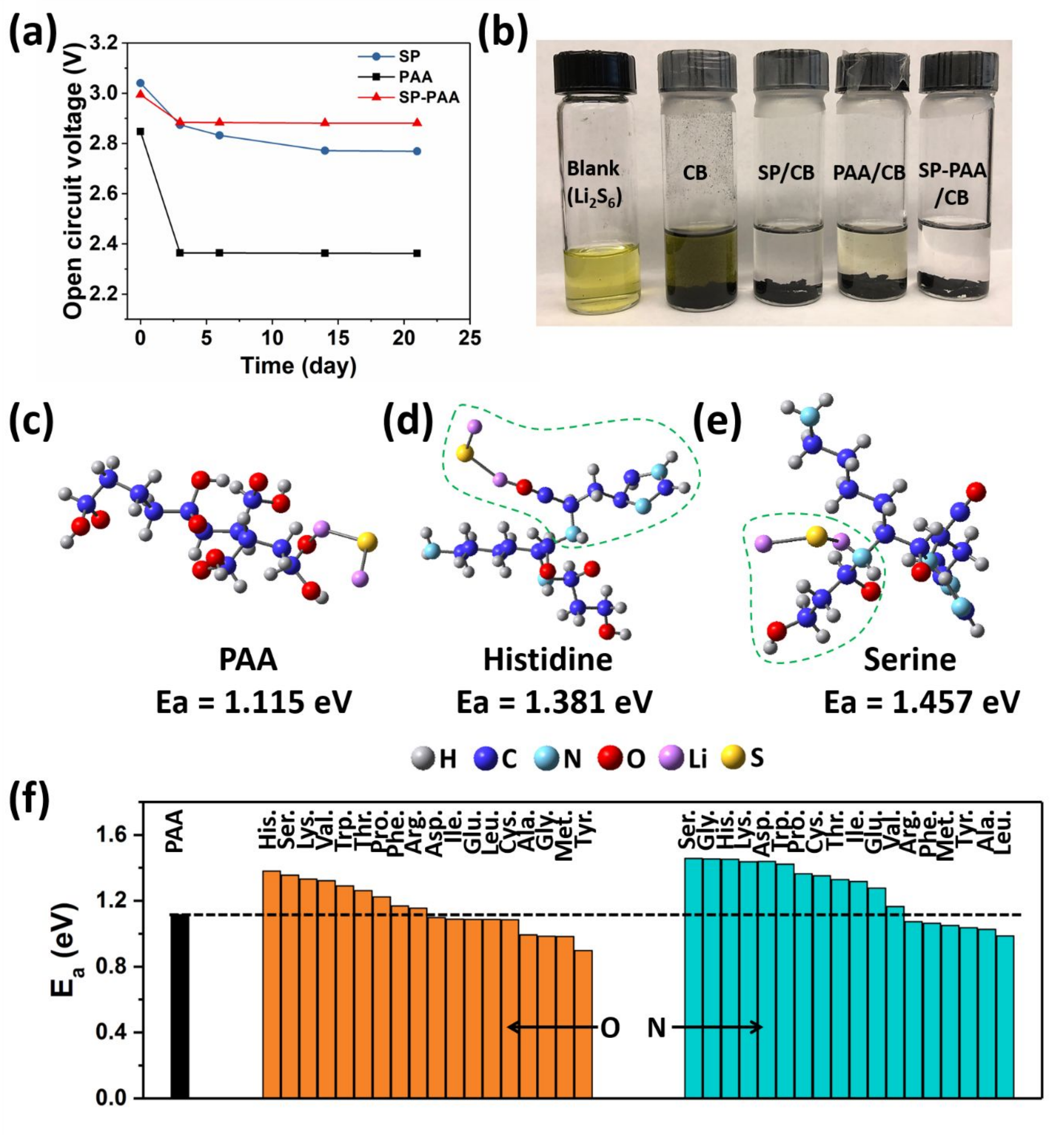

Figure 6. The ability of various binders for adsorbing polysulfides. (a) Open-circuit voltage (OCV) of S cathodes with different binders. (b) Photographs showing various composites of binder/CB in Li_2S_6 solution. (c) Optimized geometries and adsorption binding energy (Ea) of Li_2S adsorbed by PAA. (d) Optimized geometries and Ea of Li_2S adsorbed by Histidine via oxygen atom. (e) Optimized geometries and Ea of Li_2S adsorbed by Serine via nitrogen atom. (f) Summary

on the adsorption binding energies of various amino acids of SP with Li_2S via either oxygen or nitrogen atom as compared with PAA.

To further demonstrate the ability of SP-PAA to anchor polysulfides and preventing the diffusion of them, the self-discharge behavior of the S cathodes was monitored. It is well known that Li-S batteries usually suffer from severe self-discharge mainly resulting from the diffusion of polysulfides.[58,59] The open-circuit voltage (OCV) of various freshly made S cathodes was recorded with time, the decay of which can reflect the self-discharge behavior of the electrodes.[60] As shown in **Figure 6a**, the OCVs of the fresh cells with SP, PAA and SP-PAA are found to be 3.04, 2.85 and 2.99 V, respectively. After resting for 3 days, the OCVs of all cells drop down due to some diffusion of polysulfides. Specifically, the SP and SP-PAA cells present declined OCVs of 2.87 and 2.88 V, respectively. The OCV of PAA cell, however, very obviously decreases to only 2.36 V. The OCVs become steadier subsequently and after 21 days of rest, SP-PAA cell shows the highest OCV retention of 96%, while the retentions of SP and PAA cells are 91 and 83%, respectively, much lower than that of the SP-PAA cell. The result indicates that SP and SP-PAA being the binder function as effective absorbents of polysulfides to significantly reduce the self-discharge. The strong binding effect with polysulfides by SP-PAA and uniform interfaces/conduction networks among S particles and SP-PAA/CB composite should be the main reasons accounting for the smallest self-discharge of SP-PAA cell.

The digital photo in **Figure 6b** also proves the advantage of SP and SP-PAA for adsorbing polysulfides. As displayed, various composites of binder/CB with same mass were immersed in Li_2S_6 solution with DOL/DME (1 : 1 by volume) as the solvent to demonstrate the effect of different binders for adsorbing polysulfides. It is found that the addition of three types of binder/CB composites effectively adsorb polysulfides, which can be confirmed by the color change of the Li_2S_6 solution from yellow to lighter yellow or even transparent. Importantly, the polysulfide adsorption ability of SP/CB and SP-PAA/CB is much better than that of PAA/CB, due to the fact that the color of Li_2S_6 solution becomes completely transparent for them, while the solution is still yellowish for PAA/CB case.

The above results suggest that as compared with PAA, both SP and SP-PAA have stronger capability of binding polysulfides. In order to verify the polysulfide binding effect of PAA and SP, the adsorption binding energy (*Ea*) of them is calculated by using density functional theory (DFT). The schematic structures of the representative polysulfide, Li_2S, adsorbed by PAA and specific amino acids are depicted in **Figure 6c-e**, in which one active atom (O, N) is assumed to interact with one Li ion of Li_2S. In regard to PAA (**Figure 6c**), the adsorption of Li_2S is realized by carbonyl group and the binding energy is determined to be 1.115 eV. As SP possesses enormous structures and complicated amino acid sequences, to simplify the calculation of the binding energies of SP, multiple amino acid sequences with at least three different types of amino acids included in each sequence are randomly chosen, and finally 18 kinds of amino acids in total are calculated. It is also noted that as amino acid obtains both amine and carboxyl groups, O and N atoms are both taken into consideration. Take Histidine and Serine for example, **Figure 6d,e** shows the optimized geometries for adsorption of Li_2S by the amino acids via O or N atom. One finds that the binding energies of Histidine and Serine with Li_2S are 1.381 and 1.457 eV respectively, both of which are much higher than that of PAA. **Figure 6f** summarizes the adsorption binding energies of all amino acids of SP with Li_2S via O and N atoms in comparison with PAA. It is surprisingly found that a majority of amino acids such as His., Ser., Gly., Lys., Glu., Arg., etc. show much higher binding energies with Li_2S (see optimized geometries of all amino acids in

Figure S3-7). In particular, those aforementioned amino acids actually dominate the composition of SP. For instance, the contents of Glu., Asp., Arg., Lys. in SP are 19.1, 11.6, 7.6 and 6.3 wt%, respectively (the detailed amino acid profile can be found in **Table S1**). The DFT calculation results confirm that SP offers much stronger interactions with polysulfides as compared with PAA, which is consistent with experimental demonstration.

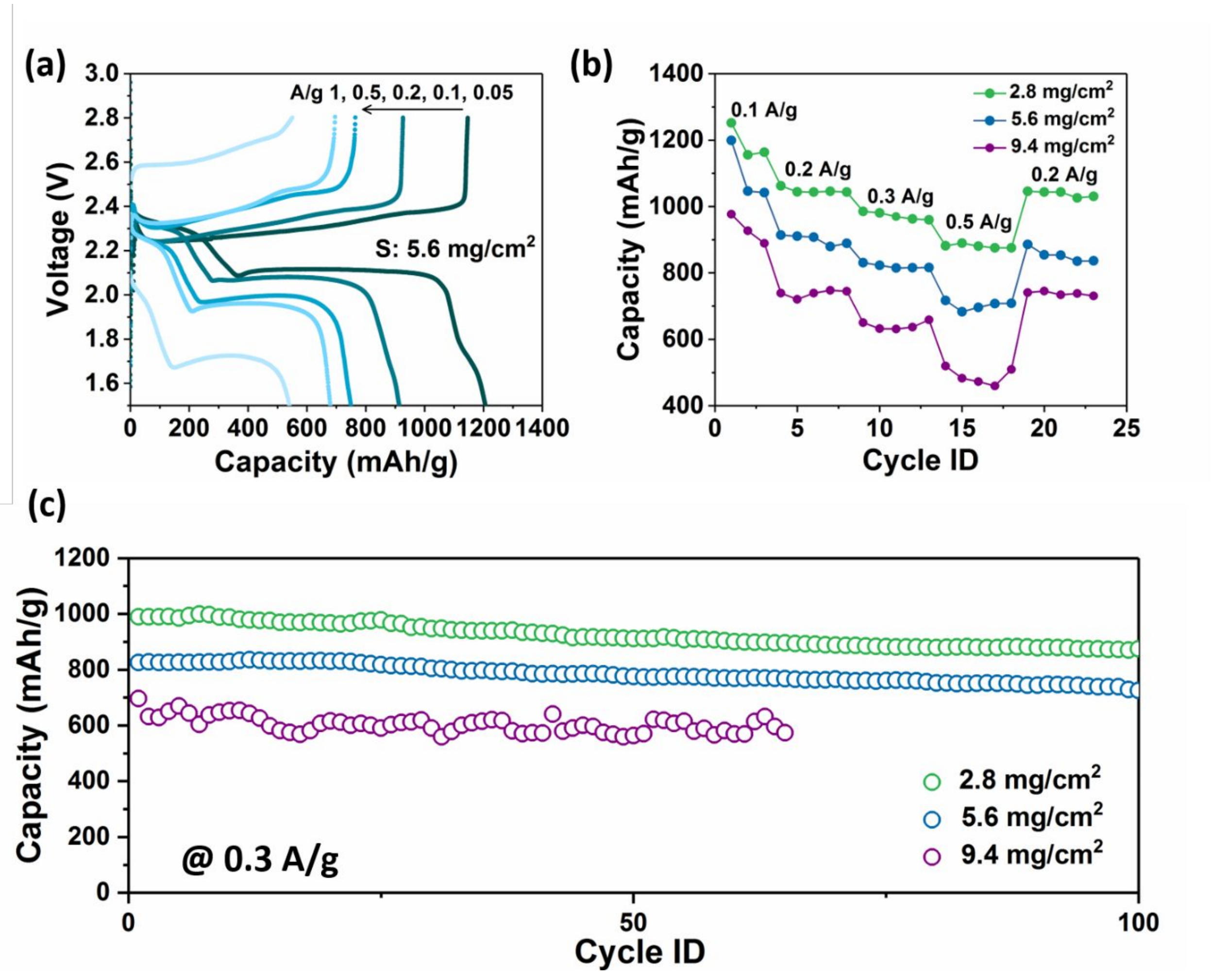

Figure 7. Electrochemical performance of Li-S batteries with high S loading. (a) Voltage profiles of S cathode with SP-PAA with a high loading of S: 5.6 mg/cm^2. (b) C-rate performance of S cathodes with SP-PAA with various loading of S. (c) Cycle stability of S cathodes with SP-PAA with various loading of S.

Aiming to achieve high-energy Li-S batteries, high loading level of S active materials is a prerequisite. In this work, therefore, we examine the high-loading S cathodes with various binders. As shown in **Figure S8**, with a higher loading of S such as ca. 2.8 mg/cm^2, all cells work normally at a small current density of 0.05 A/g. However, when enlarging the current density to 0.1 A/g, only SP-PAA cell functions well, exhibiting typical charging/discharging curves of Li-S batteries. Both SP and PAA cells fail to ensure smooth and stable electrochemical reactions, as can be reflected by the unstable voltage profiles with large polarization. It is worth noting that SP-PAA electrode is able to deliver stable performance even at a further increased S loading. As shown in **Figure 7a**, with an S loading of 5.6 mg/cm^2, the SP-PAA electrode demonstrates stable voltage profiles at various current densities. At the same time, the polarization doesn't visibly enlarge with the increasing current densities, except for the case of 1 A/g. The superior performance is contributed by the good mechanical properties, robust and porous conduction networks and effective polysulfide-confinement of SP-PAA electrode, as well as good ion-conduction of SP-PAA, which significantly assist in maintaining structural stability of the electrode and promoting the electrochemical reactions.

Figure 7b displays the C-rate performance of S cathodes with SP-PAA with various S loadings: 2.8, 5.6 and 9.4 mg/cm^2. It can be seen that the higher the loading of S, the poorer the rate performance. In other words, the S cathode with an S loading of 2.8 mg/cm^2 delivers the highest capacities over all tested current densities. In the case of 5.6 mg/cm^2 S loading, the capacities are stable over various current densities, and 97.3% capacity can be recovered when switching back the current density from 0.5 to 0.2 A/g. Furthermore, the cycle stabilities of the three electrodes at 0.3 A/g are compared in **Figure 7c**. Both electrodes with 2.8 and 5.6 mg/cm^2 active materials present very stable capacity during cycling and no obvious capacity fading can be observed.

Particularly, in the case of 5.6 mg/cm^2 loading of S, a high capacity of 826 mAh/g (areal capacity of 4.6 mAh/cm^2) is delivered and maintained as 725 mAh/g after 100 cycles. Additionally, the electrode with extremely high loading of S (9.4 mg/cm^2) exhibits a satisfactory capacity of 701 mAh/g in the beginning and retains around 610 mAh/g during cycling, corresponding to an areal capacity of 5.7 mAh/cm^2 that is much higher than commercialized lithium-ion batteries (ca. 4 mAh/cm^2)[34,61]. One still finds, however, relatively unstable capacities for such S cathode, due to the structural instability by severe volume deformation which is a critically challenging task for high-loading S cathodes.

4. Conclusions

To conclude, we have demonstrated a multi-functional binder (SP-PAA), integrating high mechanical strength, strong polysulfide adsorption and good ion-conduction ability, for realizing advanced high-energy Li-S batteries. Such multi-functional binder is fabricated by facile incorporation of two functional materials: soy protein (SP) and poly(acrylic acid) (PAA). The contributions from SP-PAA to the improvements of electrode properties/performances are systematically investigated. It is found that the synergistic effect from the combination significantly improves the microstructures (uniformity, porous structure and interfaces), adhesion property and mechanical properties of the resulting S cathode. As a result, the electrochemical performances of the S cathode (e.g. capacity, cycle stability and C-rate performance) are remarkably enhanced and the self-discharge is effectively alleviated. Importantly, the strong polysulfide binding effect by SP, which has been verified by both experimental and DFT calculation results, as well as the good ion-conduction capability of SP, make great contributions to the improved electrochemical performances. Further, high-loading S cathodes demonstrate very stable performance, due to the fact that SP-PAA can effectively maintain the structural stability of the cathode, mitigate the diffusion of polysulfides and promote the electrochemical reactions. This study provides a facile approach for developing advanced binder and high-loading S cathode via utilization of natural materials, which possesses great potential for environmental-friendly and practical applications.

ACKNOWLEDGMENTS

The authors would like to acknowledge the financial support by USDA NIFA 2015-67021-22911. The authors also thank the support on characterizations from the Franceschi Microscopy & Imaging Center, and the Composite Materials and Engineering Center at Washington State University.

References

1 C. H. Chang, S. H. Chung, P. Han and A. Manthiram, *Mater. Horizons*, 2017, **4**, 908–914.

2 L. Luo, S. H. Chung and A. Manthiram, *Adv. Energy Mater.*, 2018, **8**, 1–12.

3 H. J. Peng, J. Q. Huang, X. B. Cheng and Q. Zhang, *Adv. Energy Mater.*, 2017, **7**, 1–54.

4 W. Chen, T. Lei, T. Qian, W. Lv, W. He, C. Wu, X. Liu, J. Liu, B. Chen, C. Yan and J. Xiong, *Adv. Energy Mater.*, 2018, **8**, 1–8.

5 X. Fu, C. Li, Y. Wang, L. Scudiero, J. Liu and W. Zhong, *J. Phys. Chem. Lett.*, 2018, **9**, 2450–2459.

6 D. Lv, J. Zheng, Q. Li, X. Xie, S. Ferrara, Z. Nie, L. B. Mehdi, N. D. Browning, J. G. Zhang, G. L. Graff, J. Liu and J. Xiao, *Adv. Energy Mater.*, 2015, **5**, 1–8.

7 L. Chen and L. L. Shaw, *J. Power Sources*, 2014, **267**, 770–783.

8 C. Zhang, H. Bin Wu, C. Yuan, Z. Guo and X. W. Lou, *Angew. Chemie - Int. Ed.*, 2012, **51**, 9592–9595.

9 N. Jayaprakash, J. Shen, S. S. Moganty, A. Corona and L. A. Archer, *Angew. Chemie - Int. Ed.*, 2011, **50**, 5904–5908.

10 N. Brun, K. Sakaushi, L. Yu, L. Giebeler, J. Eckert and M. M. Titirici, *Phys Chem Chem Phys*, 2013, **15**, 6080–6087.

11 M. Rao, W. Li and E. J. Cairns, *Electrochem. commun.*, 2012, **17**, 1–5.

12 S. Wei, H. Zhang, Y. Huang, W. Wang, Y. Xia and Z. Yu, *Energy Environ. Sci.*, 2011, **4**,

736.

13 G. Li, J. Sun, W. Hou, S. Jiang, Y. Huang and J. Geng, *Nat. Commun.*, 2016, **7**, 1–10.

14 Y. Y. Hsieh, L. Zhang, D. DeArmond, S. N. Kanakaraj, P. K. Adusei, N. T. Alvarez, Y. Fang, J. Daum and V. Shanov, *Carbon*, 2018, **139**, 1093–1103.

15 X. F. Gao, J. Y. Li, D. S. Guan and C. Yuan, *ACS Appl. Mater. Interfaces*, 2014, **6**, 4154–4159.

16 W. Deng, X. Zhou, Q. Fang and Z. Liu, *ChemNanoMat*, 2016, **2**, 952–958.

17 G. Zhou, D. W. Wang, F. Li, P. X. Hou, L. Yin, C. Liu, G. Q. Lu, I. R. Gentle and H. M. Cheng, *Energy Environ. Sci.*, 2012, **5**, 8901–8906.

18 L. Sun, M. Li, Y. Jiang, W. Kong, K. Jiang, J. Wang and S. Fan, *Nano Lett.*, 2014, **14**, 4044–4049.

19 X. Fan, Y. Zhang, J. Li, K. Yang, Z. Liang, Y. Chen, C. Zhao, Z. Zhang and K. Mai, *J. Mater. Chem. A*, 2018, **6**, 11664–11669.

20 L. Ji, M. Rao, S. Aloni, L. Wang, E. J. Cairns and Y. Zhang, *Energy Environ. Sci.*, 2011, **4**, 5053.

21 S. Lu, Y. Cheng, X. Wu and J. Liu, *Nano Lett.*, 2013, **13**, 2485–2489.

22 Z. Li, J. Zhang and X. W. Lou, *Angew. Chemie - Int. Ed.*, 2015, **54**, 12886–12890.

23 S. Feng, J. Song, S. Fu, C. Zhu, Q. Shi, M. K. Song, D. Du and Y. Lin, *J. Mater. Chem. A*, 2017, **5**, 23737–23743.

24 C. Wang, K. Su, W. Wan, H. Guo, H. Zhou, J. Chen, X. Zhang and Y. Huang, *J. Mater. Chem. A*, 2014, **2**, 5018–5023.

25 J. Song, M. L. Gordin, T. Xu, S. Chen, Z. Yu, H. Sohn, J. Lu, Y. Ren, Y. Duan and D. Wang, *Angew. Chemie - Int. Ed.*, 2015, **54**, 4325–4329.

26 G. Xu, B. Ding, P. Nie, L. Shen, J. Wang and X. Zhang, *Chem. - A Eur. J.*, 2013, **19**, 12306–12312.

27 Z. Cao, J. Zhang, Y. Ding, Y. Li, M. Shi, H. Yue, Y. Qiao, Y. Yin and S. Yang, *J. Mater. Chem. A*, 2016, **4**, 8636–8644.

28 X. Li, X. Li, M. N. Banis, B. Wang, A. Lushington, X. Cui, R. Li, T. K. Sham and X. Sun, *J. Mater. Chem. A*, 2014, **2**, 12866–12872.

29 X. Fu, Y. Wang, J. Tuba, L. Scudiero and W.-H. Zhong, *Small Methods*, 2018, **2**, 1800066.

30 S. L. Chou, Y. Pan, J. Z. Wang, H. K. Liu and S. X. Dou, *Phys. Chem. Chem. Phys.*, 2014, **16**, 20347–20359.

31 J. Wang, Z. Yao, C. W. Monroe, J. Yang and Y. Nuli, *Adv. Funct. Mater.*, 2013, **23**, 1194–1201.

32 Z. Zhang, W. Bao, H. Lu, M. Jia, K. Xie, Y. Lai and J. Li, *ECS Electrochem. Lett.*, 2012, **1**,

A34–A37.

33 G. Li, W. Cai, B. Liu and Z. Li, *J. Power Sources*, 2015, **294**, 187–192.

34 W. Chen, T. Qian, J. Xiong, N. Xu, X. Liu, J. Liu, J. Zhou, X. Shen, T. Yang, Y. Chen and C. Yan, *Adv. Mater.*, 2017, **29**, 1605160.

35 M. Ling, L. Zhang, T. Zheng, J. Feng, J. Guo, L. Mai and G. Liu, *Nano Energy*, 2017, **38**, 82–90.

36 J. Liu, M. Sun, Q. Zhang, F. Dong, P. Kaghazchi, Y. Fang, S. Zhang and Z. Lin, *J. Mater. Chem. A*, 2018, **6**, 7382–7388.

37 M. Ling, W. Yan, A. Kawase, H. Zhao, Y. Fu, V. S. Battaglia and G. Liu, *ACS Appl. Mater. Interfaces*, 2017, **9**, 31741–31745.

38 H. Su, C. Fu, Y. Zhao, D. Long, L. Ling, B. M. Wong, J. Lu and J. Guo, *ACS Energy Lett.*, 2017, **2**, 2591–2597.

39 Z. Fanglei, W. Weikun, W. Anbang, Y. Keguo, J. Zhaoqing and Y. Yu-sheng, *ACS Appl. Mater. Interfaces*, 2015, **7**, 26257–26265.

40 L. Yan, X. Gao, J. P. Thomas, J. Ngai, H. Altounian, K. T. Leung, Y. Meng and Y. Li, *Sustain. Energy Fuels*, 2018, **2**, 1574–1581.

41 Z. Yang, R. Li and Z. Deng, *ACS Appl. Mater. Interfaces*, 2018, **10**, 13519–13527.

42 F. L. Zeng, N. Li, Y. Q. Shen, X. Y. Zhou, Z. Q. Jin, N. Y. Yuan, J. N. Ding, A. B. Wang, W. K. Wang and Y. S. Yang, *Energy Storage Mater.*, 2018, 1–9.

43 H. Souzandeh, K. S. Johnson, Y. Wang, K. Bhamidipaty and W.-H. Zhong, *ACS Appl. Mater. Interfaces*, 2016, **8**, 20023–20031.

44 L. Yan, X. Gao, F. Wahid-Pedro, J. T. Ernest Quinn, Y. Meng and Y. Li, *J. Mater. Chem. A*, 2018, **6**, 14315–14323.

45 Z. W. Seh, Y. Sun, Q. Zhang and Y. Cui, *Chem. Soc. Rev.*, 2016, **45**, 5605–5634.

46 K. Nishinari, Y. Fang, S. Guo and G. O. Phillips, *Food Hydrocoll.*, 2014, **39**, 301–318.

47 X. Fu, Y. Jewel, Y. Wang, J. Liu and W.-H. Zhong, *J. Phys. Chem. Lett.*, 2016, 4304–4310.

48 S. S. Zhang, D. T. Tran and Z. Zhang, *J. Mater. Chem. A*, 2014, **2**, 18288–18292.

49 W. Kam, C. W. Liew, J. Y. Lim and S. Ramesh, *Ionics*, 2014, **20**, 665–674.

50 Z. Tai, J. Yang, Y. Qi, X. Yan and Q. Xue, *RSC Adv.*, 2013, **3**, 12751–12757.

51 H. Tian, G. Xu, B. Yang and G. Guo, *J. Food Eng.*, 2011, **107**, 21–26.

52 K. Li, S. Jin, H. Chen, J. He and J. Li, *Polymers,* 2017, **9,** 167.

53 J. Liu, D. G. D. Galpaya, L. Yan, M. Sun, Z. Lin, C. Yan, C. Liang and S. Zhang, *Energy Environ. Sci.*, 2017, **10**, 750–755.

54 X. Wang, X. Fu, Y. Wang and W. Zhong, *Polym. (United Kingdom)*, 2016, **106**, 43–52.

55 X. Fu, C. Li, Y. Wang, L. P. Kovatch, L. Scudiero, J. Liu and W. Zhong, *ACS Appl. Mater. Interfaces*, 2018, **10**, 4726–4736.

56 N. Ding, L. Zhou, C. Zhou, D. Geng, J. Yang, S. W. Chien, Z. Liu, M. F. Ng, A. Yu, T. S. A. Hor, M. B. Sullivan and Y. Zong, *Sci. Rep.*, 2016, **6**, 1–10.

57 X. Fu, Y. Wang, L. Scudiero and W. H. Zhong, *Energy Storage Mater.*, 2018, **15**, 447–457.

58 S. H. Chung and A. Manthiram, *ACS Energy Lett.*, 2017, **2**, 1056–1061.

59 L. Wang, J. Liu, S. Yuan, Y. Wang and Y. Xia, *Energy Environ. Sci.*, 2016, **9**, 224–231.

60 L. Wang, Y. B. He, L. Shen, D. Lei, J. Ma, H. Ye, K. Shi, B. Li and F. Kang, *Nano Energy*, 2018, **50**, 367–375.

61 S. Urbonaite, T. Poux and P. Novák, *Adv. Energy Mater.*, 2015, **5**, 1500118.